PAPER

Electronic, magnetic and structural properties of CoFeVAI and CoFeV $_{0.5} \mathrm{Mn}_{0.5} \mathrm{AI}$

To cite this article: Parashu Kharel et al 2024 J. Phys. D: Appl. Phys. 57 375001

View the article online for updates and enhancements.

You may also like

- Effect of the Synthesis Conditions on the Preparation and Electrochemical Properties of LiNi0.5Mn0.5O2 Made by Ion Exchange
- Jordi Cabana and Clare Grey
- Metallic Nanoparticles and Proton Conductivity: Improving Proton Conductivity of BaCe_{0.9}Y_{0.4}O₃ and La_{0.75}Sr_{0.25}Cr_{0.5}Mn_{0.5}O₃ by Ni-doping Maria Teresa Caldes, Kostian V. Kravchyk, Messaoud Benamira et al.
- <u>Lithium De-intercalation Mechanism in</u> <u>LiNi0.5Mn0.5O2</u> Yang Shao-Horn, Sundeep Kumar, Ying Meng et al.





J. Phys. D: Appl. Phys. 57 (2024) 375001 (10pp)

https://doi.org/10.1088/1361-6463/ad5696

Electronic, magnetic and structural properties of CoFeVAI and CoFeV_{0.5}Mn_{0.5}AI

Parashu Kharel¹, Gavin Baker¹, Matthew Wieberdink¹, Salimatou Diallo², Mohd Anas¹, Paul M Shand² and Pavel V Lukashev^{2,*}

E-mail: pavel.lukashev@uni.edu

Received 30 April 2024 Accepted for publication 11 June 2024 Published 20 June 2024



Abstract

In this study, we present results of a comprehensive computational and experimental study of CoFeVAl and CoFeV $_{0.5}$ Mn $_{0.5}$ Al Heusler alloys. It is shown that while CoFeVAl exhibits a fairly large degree of spin polarization, this material is not half-metallic due to the presence of the vanadium spin-down states at the Fermi level. However, replacing 50% of vanadium with manganese results in a nearly half-metallic transition, largely due to the shift of the Fermi level towards occupied states. Moreover, the half-metallicity of CoFeV $_{0.5}$ Mn $_{0.5}$ Al is rather robust in a wide range of considered mechanical strain and under experimentally observed B2-type atomic disorder, thus making this alloy potentially suitable for practical spintronic applications. Both considered alloys exhibit ferromagnetic alignment at larger lattice constants, aside from a relatively small magnetic moment of vanadium which is anti-aligned with the magnetic moments of Co, Fe and Mn. We have synthesized both CoFeVAl and CoFeV $_{0.5}$ Mn $_{0.5}$ Al alloys in cubic structure with some structural disorder using arc melting and annealing. The structural and magnetic properties of the synthesized CoFeV $_{0.5}$ Mn $_{0.5}$ Al alloy are in good agreement with the theoretical calculations but vary slightly from the parent compound.

Keywords: half metals, Heusler alloys, spintronics

1. Introduction

Among various materials studied for applications in spin-based electronics (spintronics), Heusler alloys attracted particular attention, in part due to their relative ease of fabrication, simple crystal structure, high tunability and high Curie temperature [1–5]. More specifically, Heusler alloys have been studied for decades as potential half-metallic and, more recently, spin-gapless semiconducting systems. Half-metals are materials that are electric conductors for one of the electron spins and insulators for the opposite spin making them 100% spin-polarized. The degree of spin polarization (*P*) is defined

as $P = \frac{N_{\uparrow}(E_F) - N_{\downarrow}(E_F)}{N_{\uparrow}(E_F) + N_{\downarrow}(E_F)}$, where $N_{\uparrow\downarrow}(E_F)$ is the spin-dependent density of states at the Fermi level, E_F [6]. Similarly, spin-gapless semiconductors (SGSs) are materials that are insulating for one spin and gapless semiconductors for the opposite spin. Half-metallic materials were predicted by de Groot *et al* [7]. This seminal work resulted in intense studies of various potentially half-metallic systems. Many of these systems have been investigated theoretically, while some have been experimentally synthesized and characterized [8–11]. The investigation of half-metallic Heusler alloys has reached a considerable level of maturity, which is obvious from the number of peerreviewed articles in circulation [12–14]. SGSs have been theoretically predicted by Wang in 2008 [15]. However, this field of research is advancing very slowly mainly because of difficulty in synthesizing Heusler alloys exhibiting SGS properties.

¹ Department of Chemistry, Biochemistry and Physics, South Dakota State University, Brookings, SD 57007, United States of America

² Department of Physics, University of Northern Iowa, Cedar Falls, IA 50614, United States of America

^{*} Author to whom any correspondence should be addressed.

The electronic structure of potential SGS materials is very sensitive to various external influences, such as mechanical pressure and different forms of defects and impurities [16–18].

The electronic band properties of Heusler alloys can be modified by external factors, such as mechanical strain and atomic substitution/doping [19-26]. In thin film structures, interface engineering has also been used to tune and restore half-metallic properties [27–30]. In this paper, we consider the effect of both mechanical strain and atomic substitution on structural, electronic and magnetic properties of the quaternary Heusler compound CoFeVAl. In particular, our results indicate that while CoFeVAl exhibits a large degree of spin polarization, the alloy is not half-metallic, due to the presence of vanadium spin-down states at the Fermi level. However, replacing 50% of vanadium with manganese results in a halfmetallic transition, largely due to the shift of the Fermi level towards occupied states. Further, the CoFeV_{0.5}Mn_{0.5}Al alloy retains its half-metallic properties over a relatively large range of considered mechanical strain and also under B2-type atomic disorder, making this alloy potentially attractive for spintronic device applications.

The rest of the paper is organized as follows. In section 2, we outline the computational and experimental methods. The main results, both computational and experimental, are presented in section 3. The computational sub-section consists of three parts, namely, ground state properties, effect of mechanical strain and effect of atomic disorder. Section 4 contains concluding remarks, followed by acknowledgments to funding sources and computational facilities.

2. Methods

2.1. Computational methods

The computational results reported in this article are obtained using the Vienna ab initio simulation package [31]. All calculations are performed using the projector augmentedwave method [32] and generalized-gradient approximation [33]. The integration method by Methfessel and Paxton [34] is employed, with a cut-off energy of 500 eV. We used the k-point mesh of $12 \times 12 \times 12$ for the Brillouinzone integration. The energy convergence criterion is set to 10^{-3} meV. The biaxial strain is imposed by fixing the in-plane and relaxing the out-of-plane lattice parameters, i.e. by allowing the system to exhibit tetragonal symmetry. Some of the input files are set up with the MedeA® software environment [35]. All calculations are performed using the Advanced Cyberinfrastructure Coordination Ecosystem: Services & Support (formerly known as Extreme Science and Engineering Discovery Environment) resources located at the Pittsburgh Supercomputing Center [36] and with the resources of the Center for Functional Nanomaterials at Brookhaven National Laboratory.

2.2. Experimental methods

The bulk ingots of both CoFeVAl and CoFeV_{0.5}Mn_{0.5}Al alloys were prepared using arc melting and annealing. The CoFeVAl

ingot was synthesized by melting together small pieces of Co, Fe, V and Al cut from commercially available metal pellets matching the expected stoichiometry. These metal pellets were at least 99.95% pure. The melting process was carried out on a water-cooled copper crucible of an arc furnace in a continuous flow of argon gas. The same procedure was used while preparing CoFeV_{0.5}Mn_{0.5}Al. The arcmelted ingots were sealed in quartz tubes under partial argon pressure and annealed at 850 °C for 72 h. The elemental compositions of the annealed samples were determined using energy-dispersive x-ray spectroscopy. The average elemental compositions of these samples are Co_{0.90}Fe_{0.99}V_{1.0}Al_{1.11} and $Co_{1.03}Fe_{0.98}V_{0.53}Mn_{0.46}Al_{1.00}$, which are close to the nominal compositions CoFeVAl and CoFeV_{0.5}Mn_{0.5}Al, respectively. The crystal structures of the alloys were investigated by analyzing the x-ray diffraction (XRD) patterns recorded from powder samples made of the annealed ingots. The fine powder samples were prepared by crushing the annealed ingots using mortar and pestle. The x-ray patterns were recorded at room temperature using a Rigaku Miniflex600 diffractometer. The Rietveld refinement of the powder XRD data was carried out using the FullProf suite [37]. The magnetic measurements were performed using magnetometers on the Quantum Design VersaLab and Dynacool PPMS platforms.

3. Results and discussion

3.1. Computational results

3.1.1. Ground state properties. Our calculations indicate that the lowest energy structure for CoFeVAI is the cubic Y structure (space group F-43m) with Co, Fe, V and Al occupying (1/4,1/4,1/4), (3/4,3/4,3/4), (1/2,1/2,1/2) and (0,0,0) Wyckoff atomic positions. We also examined alternative configurations of Co, Fe and V within the cubic Y structure; however, these arrangements resulted in higher equilibrium energies and are not discussed further in this paper.

Figure 1(a) shows calculated energy (black line and squares) and magnetization (blue line and circles) of CoFeVAI under uniform pressure, as a function of lattice constant. The calculated ground state lattice parameter is $a=5.718\text{\AA}$, with the corresponding magnetization value of $m=0.955\,\mu_{\rm B}/f.u.$ Figure 1(b) shows the calculated element-resolved density of states of CoFeVAI at the optimal lattice constant. The magnetization of CoFeVAI is sensitive to the lattice parameter. As shown in figure 1(a), the magnetization expressed in units of $\mu_{\rm B}/f.u$ decreases with a decrease in lattice parameter below its equilibrium value; while the magnetization remains almost constant around $0.95-0.96\,\mu_{\rm B}/f.u.$ despite the increase in the lattice parameter above its equilibrium value. This issue will be further discussed below.

The calculated spin polarization of CoFeVAl at the optimal lattice constant is 87%. A close inspection of figure 1(b) shows that this value could be significantly higher (essentially resulting in half-metallic electronic structure) if a relatively small number of spin-down vanadium states (green line) were absent around the Fermi level. Thus, there is a possibility that reducing the vanadium content by replacing it with another

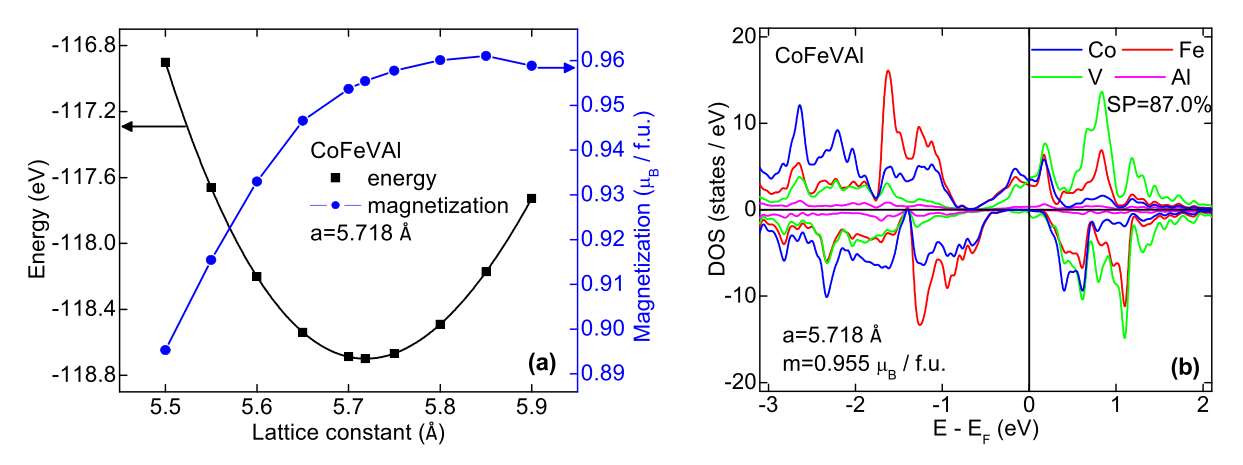


Figure 1. (a) Calculated energy (black line and squares) and magnetization (blue line and circles) of CoFeVAl under uniform pressure, as a function of lattice constant. (b) Calculated density of states of CoFeVAl at the optimal lattice parameter. Elemental contributions are colored as indicated in the figure. The vertical line corresponds to the Fermi level. Positive/negative DOS represents spin-up/spin-down states, correspondingly.

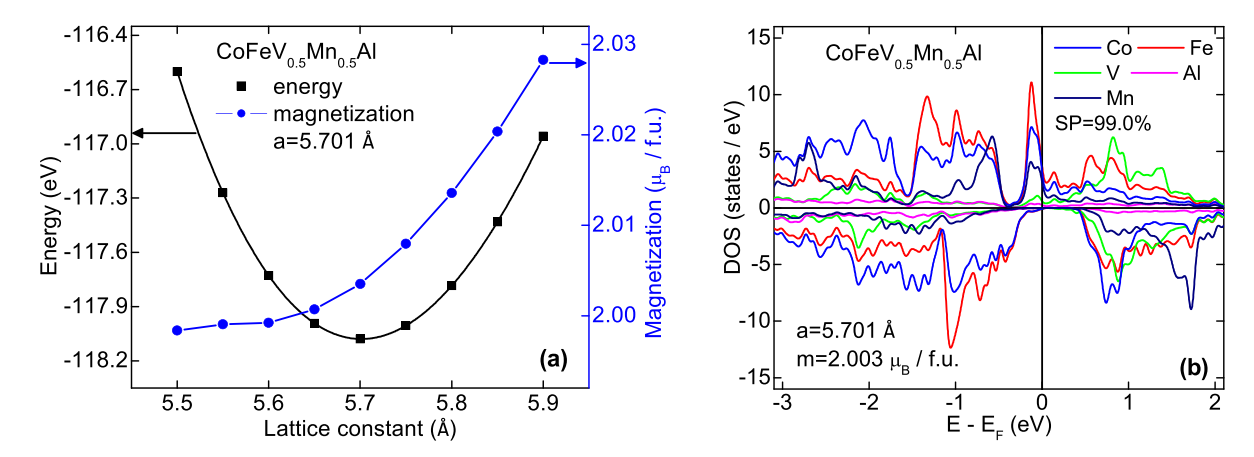


Figure 2. (a) Calculated energy (black line and squares) and magnetization (blue line and circles) of CoFeV_{0.5}Mn_{0.5}Al under uniform pressure, as a function of lattice constant. (b) Calculated density of states of CoFeV_{0.5}Mn_{0.5}Al at the optimal lattice parameter. Elemental contributions are colored as indicated in the figure. The vertical line corresponds to the Fermi level. Positive/negative DOS represents spin-up/spin-down states, correspondingly.

element could induce half-metallicity. With this in mind, we analyzed the electronic structure of CoFeV_{0.5}Mn_{0.5}Al as discussed below.

Figure 2(a) shows the calculated energy (black line and squares) and magnetization (blue line and circles) of CoFeV_{0.5}Mn_{0.5}Al under uniform pressure, as a function of lattice constant. The calculated ground state lattice parameter is a = 5.701Å, with the corresponding magnetization value of $m = 2.003 \mu_B/f.u$. This magnetization is slightly more than double the value calculated for the parent alloy. Figure 2(b) shows calculated element-resolved density of states of CoFeV_{0.5}Mn_{0.5}Al at the optimal lattice constant. The calculated value of spin polarization is 99%, meaning this alloy is essentially half-metallic in the ground state. The magnetization of CoFeV_{0.5}Mn_{0.5}Al is relatively constant under the compression of the cell, while for the expansion of the cell it exhibits a slight increase from around $2.00\mu_B/f.u.$ to $2.03\mu_{\rm B}/f.u.$, figure 2(a). We will discuss the behavior of magnetization of both CoFeVAl and CoFeV_{0.5}Mn_{0.5}Al in more detail below.

To get further insight into the nature of half-metallic transition upon substitution of 50% of V with Mn, we plot the zoomed version of DOS plots for spin-down states of CoFeVAl and CoFeV_{0.5}Mn_{0.5}Al, see figure 3. As seen in this figure, replacement of 50% of V with Mn results in a significant shift (~0.3 eV) of the Fermi level towards the occupied states. In addition, the number of spin-down V states around Fermi level reduces with 50% V replacement, which is probably a trivial result (50% less vanadium, hence less V states). Overall, it appears that the half-metallic transition in CoFeV_{0.5}Mn_{0.5}Al is largely due to the shift of the Fermi level towards occupied states as compared with the parent compound.

3.1.2. Effect of mechanical strain. Figures 4(A) and (B) respectively show the calculated total density of states of CoFeVAl and CoFeV $_{0.5}$ Mn $_{0.5}$ Al under uniform pressure, for different values of lattice parameters as indicated in the figure. The calculated spin polarization values for each of the lattice constants are also shown. As is apparent from the figure,

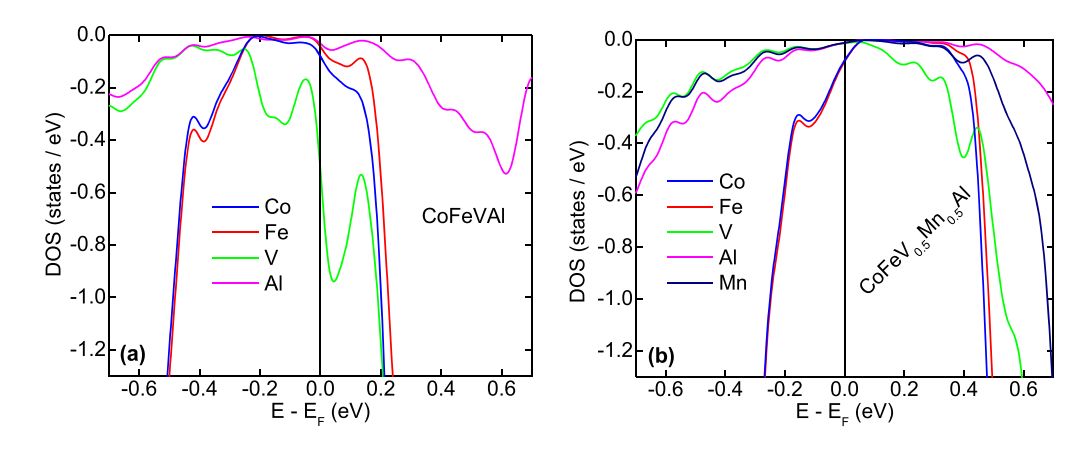


Figure 3. (a) Zoomed versions of DOS plots for spin-down states of CoFeVAl (a) and CoFeV $_{0.5}$ Mn $_{0.5}$ Al (b), calculated at the equilibrium lattice constants. Elemental contributions are colored as indicated in the figure. The vertical line corresponds to the Fermi level.

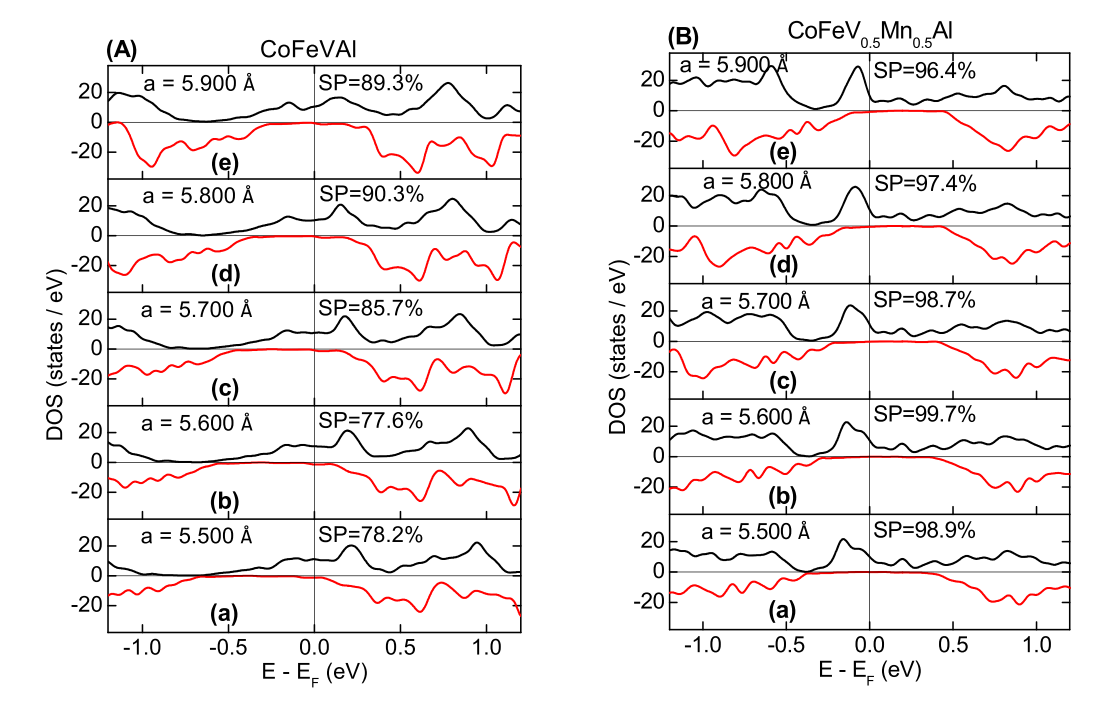


Figure 4. Calculated total density of states of CoFeVAl (A) and CoFeV_{0.5}Mn_{0.5}Al (B) for different values of lattice parameters (indicated in the figure) calculated at uniform pressure. The vertical line corresponds to the Fermi level. Positive (black line)/negative (red line) DOS represents spin-up/spin-down states, correspondingly. Calculated spin polarization values for each lattice constant are shown in the figure.

the spin polarization values of CoFeV_{0.5}Mn_{0.5}Al are not very sensitive to variation of the lattice parameter, whereas those of CoFeVAl are somewhat sensitive. In particular, the increase of the unit cell volume results in an increase of the spin polarization of CoFeVAl from around 80% to around 90% (from the smallest to the largest considered lattice constant), while the spin polarization of CoFeV_{0.5}Mn_{0.5}Al is relatively constant (remains above 96%) in the entire range of the considered lattice parameters. The small decrease in spin polarization of CoFeV_{0.5}Mn_{0.5}Al as the lattice parameter increases is caused by the shift of the spin-down valence band maximum towards the Fermi level

Figures 5(a) and (b) respectively show the calculated element-resolved magnetic moments of CoFeVAl and CoFeV_{0.5}Mn_{0.5}Al under uniform pressure, as a function of

lattice constant. The magnetic moments per atom for different elements are represented by different colors. As is clear from the figure, both CoFeVAl and CoFeV_{0.5}Mn_{0.5}Al are ferromagnetic, aside from a relatively small magnetic moment of vanadium which is anti-aligned with the magnetic moments of Co, Fe and Mn. For CoFeVAl, the magnetic moments of both Co and Fe increase with the increase of the lattice parameter, while the magnetic moment of V decreases. Overall, this results in an initial increase and subsequent saturation of the magnetization with the lattice constant, as shown in figure 1(a). As for CoFeV_{0.5}Mn_{0.5}Al, the dominant feature shown in figure 5(b) is the increase of the magnetic moment of Mn with the increase of the lattice constant; the magnetic moments of other elements are less sensitive to the change of the unit cell volume. This results in an overall increase of

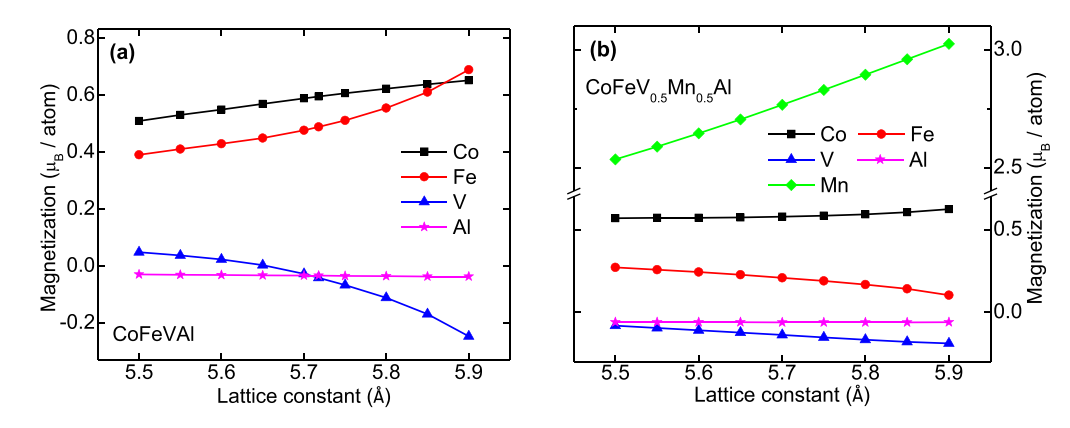


Figure 5. Calculated element-resolved magnetic moments of CoFeVAl (a) and CoFeV_{0.5}Mn_{0.5}Al (b) as a function of lattice constant, calculated at uniform pressure. The magnetic moments per elements are colored/labeled as indicated in the figure and are as follows: black line and squares—Co, red line and circles—Fe, blue line and triangles—V, magenta line and stars—Al, green line and rhombuses—Mn.

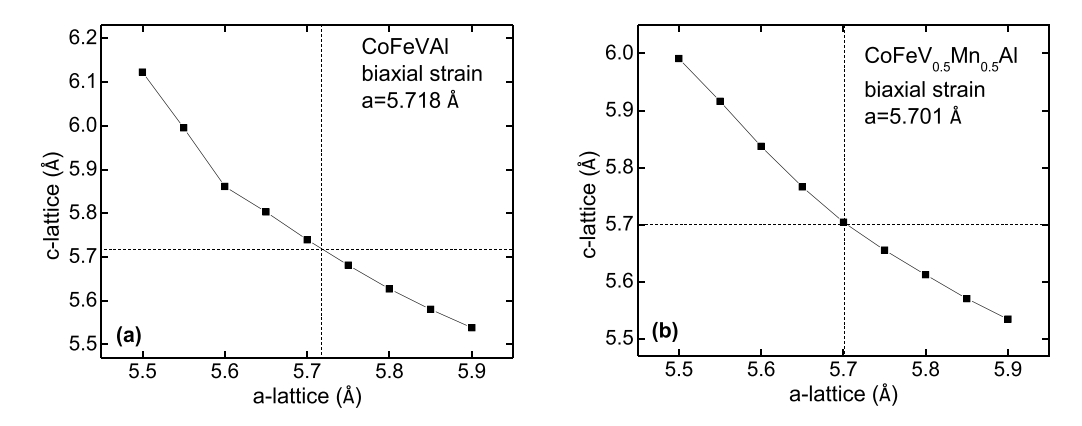


Figure 6. Calculated out-of-plane (*c*-lattice) vs. in-plane (*a*-lattice) lattice parameters of CoFeVAl (a) and CoFeV_{0.5}Mn_{0.5}Al (b) under biaxial strain

the magnetization of CoFeV_{0.5}Mn_{0.5}Al as the unit cell volume is increased, as shown in figure 2(a). However, as shown in figures 1(a) and 2(a), the effect of uniform pressure on the magnetization of both CoFeVAl and CoFeV_{0.5}Mn_{0.5}Al is relatively moderate (less than $0.1\mu_{\rm B}/f.u.$ change) in the entire range of the considered strain.

In addition to uniform pressure, we also analyzed the behavior of CoFeVAl and CoFeV_{0.5}Mn_{0.5}Al under biaxial strain, which is a more realistic scenario in practical implementations, e.g. in thin-film applications. Figure 6 shows calculated out-of-plane lattice constant (*c*-lattice) as a function of in-plane lattice constant (*a*-lattice) for CoFeVAl (a) and CoFeV_{0.5}Mn_{0.5}Al (b). The c-over-a plots for both alloys are nearly linear, except for the two smallest in-plane lattice constants of CoFeVAl. This deviation from non-linearity is likely non-physical, as elaborated in the next two paragraphs.

Figures 7(A) and (B) respectively show the calculated total density of states of CoFeVAl and CoFeV $_{0.5}$ Mn $_{0.5}$ Al under biaxial strain, for different values of in-plane lattice parameters as indicated in the figure. The calculated spin polarization values for each of the lattice constants are also shown. Similar to the case of uniform pressure, the spin polarization values of CoFeV $_{0.5}$ Mn $_{0.5}$ Al are not very sensitive to variation of the

lattice parameter, i.e. the tetragonal distortion does not result in decrease of the spin polarization. At the same time, the spin polarization of CoFeVAl is also more or less constant over the entire range of the considered biaxial strain, except for the smallest in-plane lattice constant, at which the system becomes non-spin-polarized. This result is probably non-physical, since under such a strong distortion of the unit cell volume the system is unlikely to be realized experimentally.

Figures 8(a) and (b) respectively show the calculated element-resolved magnetic moments of CoFeVAl and CoFeV_{0.5}Mn_{0.5}Al under biaxial strain, as a function of inplane lattice constant. The magnetic moments per atom for different elements are represented by different colors. Consistent with the results presented above, both CoFeVAl and CoFeV_{0.5}Mn_{0.5}Al are ferromagnetic, aside from a relatively small magnetic moment of vanadium which is antialigned with the magnetic moments of Co, Fe and Mn. As seen in figure 8(a), at the smallest considered in-plane lattice parameters, the magnetic moments of Co and Fe essentially vanish. This agrees with the non-spin-polarized nature of this alloy at the smaller considered lattice constant (figure 7(A-a) and likely represents a non-physical behavior, as discussed above.

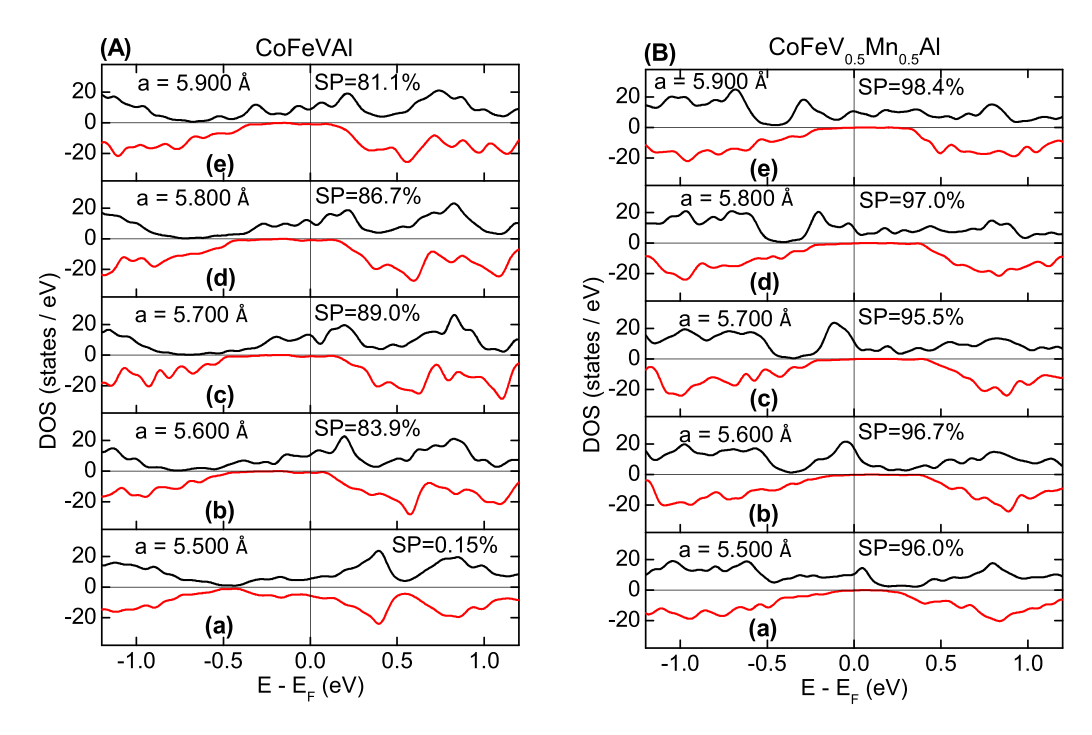


Figure 7. Calculated total density of states of CoFeVAl (A) and CoFeV_{0.5}Mn_{0.5}Al (B) for different values of lattice parameters (indicated in the figure) calculated under biaxial strain. The vertical line corresponds to the Fermi level. Positive (black line)/negative (red line) DOS represents spin-up/spin-down states, correspondingly. Calculated spin polarization values for each lattice constant are shown in the figure.

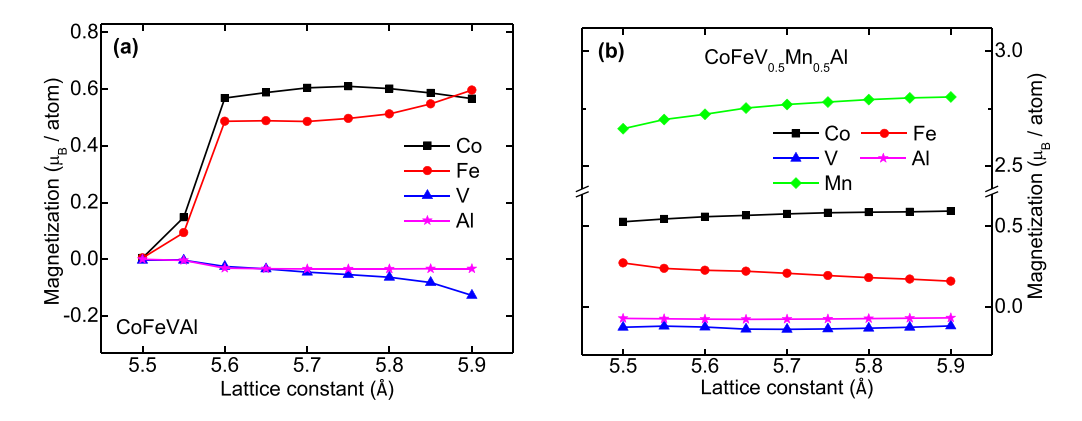


Figure 8. Calculated element-resolved magnetic moments of CoFeVAl (a) and CoFeV_{0.5}Mn_{0.5}Al (b) as a function of lattice constant, calculated under biaxial strain. The magnetic moments per elements are colored/labeled as indicated in the figure and are as follows: black line and squares—Co, red line and circles—Fe, blue line and triangles—V, magenta line and stars—Al, green line and rhombuses—Mn.

3.1.3. Effect of atomic disorder. The results presented above correspond to the ideal cubic Y-type crystal structure, which can rarely be realized in practice. Therefore, we also analyzed the effect of two types of atomic disorder that are commonly reported in Heusler compounds. In particular, as explained in the experimental section below, our CoFeVAl and CoFeV_{0.5}Mn_{0.5}Al samples respectively exhibit A2 and B2 types of atomic disorder. The former corresponds to a random mixing of atoms in the cell, while the latter corresponds to the exchange of Y and Z atoms in XX'YZ quaternary systems. Thus, to simulate B2 disorder, we interchanged the positions of one of the V and Al atoms in the CoFeV_{0.5}Mn_{0.5}Al unit cell. Simulating A2-type disorder is significantly more difficult. However, to get a rough idea of the effect of this disorder on the properties of CoFeVAl, we considered two possible configurations. First, we replaced the position of one atom of Co with V and one atom of Fe with Al. Second, we replaced the position of one atom of Fe with V and one atom of Co with Al. The second configuration has slightly lower energy, so we used it for calculating the electronic and magnetic properties of the A2-disordered cell. The results of these calculations are shown in figure 9.

As is apparent from figure 9, while the A2-type disorder has a detrimental effect on the spin polarization of CoFeVAI, the electronic structure of CoFeV $_{0.5}$ Mn $_{0.5}$ Al is almost insensitive to the B2-type disorder. In particular, B2-disordered CoFeV $_{0.5}$ Mn $_{0.5}$ Al retains its half-metallic properties and integer magnetization of $2.00\mu_{\rm B}/f.u$. While the magnetization of A2-type disordered CoFeVAI increases to around $2.41\mu_{\rm B}/f.u$., the spin polarization is reduced to around 29%.

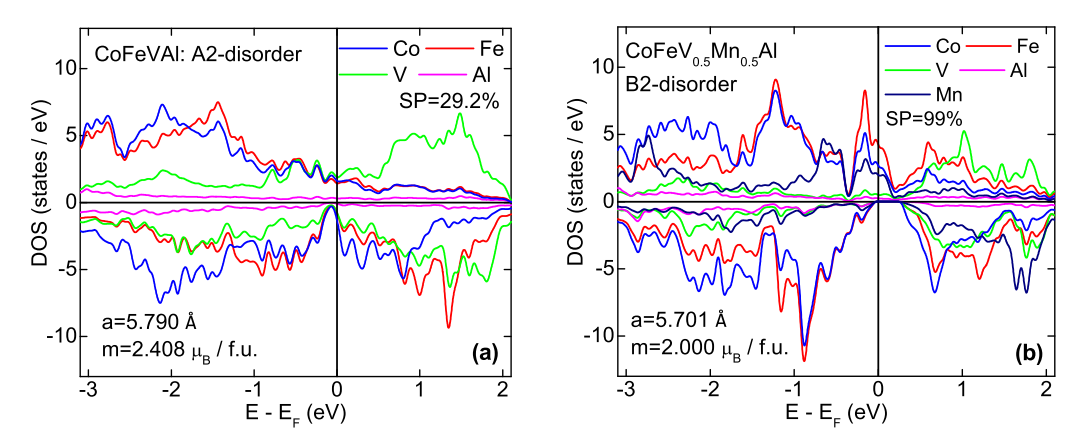


Figure 9. Calculated density of states of CoFeVAl with A2-type disorder (a) and that of $CoFeV_{0.5}Mn_{0.5}Al$ with B2-type disorder (b) at their optimal lattice parameters. Elemental contributions are colored as indicated in the figure. The vertical line corresponds to the Fermi level. Positive/negative DOS represents spin-up/spin-down states, correspondingly. Calculated spin polarization and magnetization values are shown in the figure.

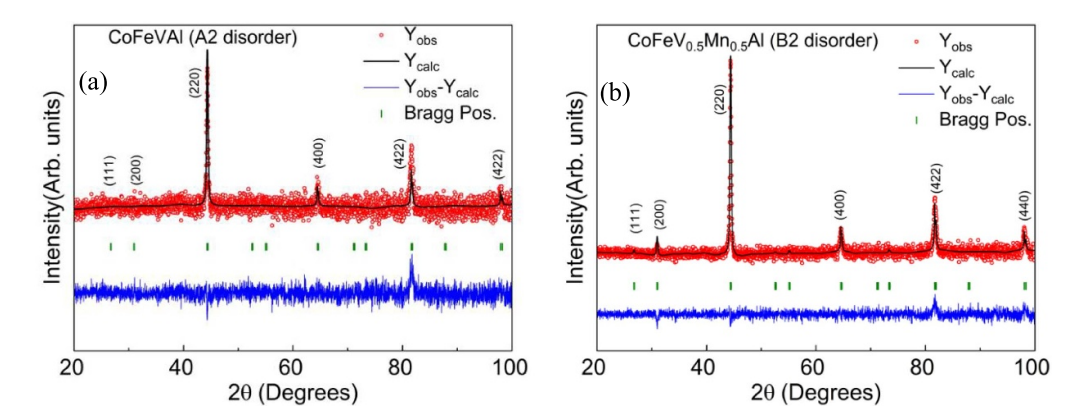


Figure 10. The room temperature powder x-ray diffraction patterns and corresponding Rietveld refined patterns of CoFeVAl and CoFeV $_{0.5}$ Mn $_{0.5}$ Al are shown in figures (a) and (b), respectively.

We emphasize here, however, that the presented results for A2-disordered cell may be sensitive to a particular atomic arrangement, of which only two representative cases are considered in this work, as explained above. A more detailed study of all possible disorder configurations goes beyond the scope of this work, but the presented results of reduced spin polarizations may serve as another indication that CoFeV_{0.5}Mn_{0.5}Al is a more appealing compound for practical applications than CoFeVAl.

3.2. Experimental results

The room temperature powder XRD patterns of CoFeVAl and CoFeV_{0.5}Mn_{0.5}Al are shown in figure 10. Both the patterns are indexed with a single-phase cubic structure with some disorder. The lack of both (111) and (200) peaks indicate that CoFeVAl contains A2 type disorder, whereas the pattern of CoFeV_{0.5}Mn_{0.5}Al lacks only the (111) peak expected for a completely ordered phase, indicating that it contains B2 type disorder. The lattice parameters obtained from the Rietveld refinement of XRD patterns of CoFeVAl and CoFeV_{0.5}Mn_{0.5}Al are respectively 5.7767(20) Å and 5.7709(8) Å which agree well with the ground state lattice

parameters estimated from our first principles calculations as mentioned in section 3.1 above. The small decrease in the lattice parameter due to Mn doping is observed both in calculation and experiment. The refinement was carried out using the space group F-43m. The atomic positions were the same as mentioned in section 3.1. However, the site occupancies were varied to get better fit with the experimental data. Both the original and the Rietveld refined XRD patterns are shown in figure 10. The degree of B2 ordering expressed in terms of the ordering parameter S_{B2} in $CoFeV_{0.5}Mn_{0.5}Al$ has been calculated using the intensities of (200) and (220) peaks, which is about 0.92, i.e. 92% ordering [38].

Figure 11(a) shows the temperature dependence of magnetization M(T) of CoFeV_{0.5}Mn_{0.5}Al measured between 5 K and 600 K and its inset shows the corresponding curve of CoFeVAl measured between 5 K and 350 K. Both the alloys show a gradual change in magnetization indicating a transition from the ferromagnetic to paramagnetic phase as they approach their respective Curie temperatures. The Curie temperatures determined from the dM/dT versus T plots are 30 K and 454 K for CoFeVAl and CoFeV_{0.5}Mn_{0.5}Al, respectively.

In order to understand the nature of magnetic ordering in these materials, we have plotted inverse susceptibility as

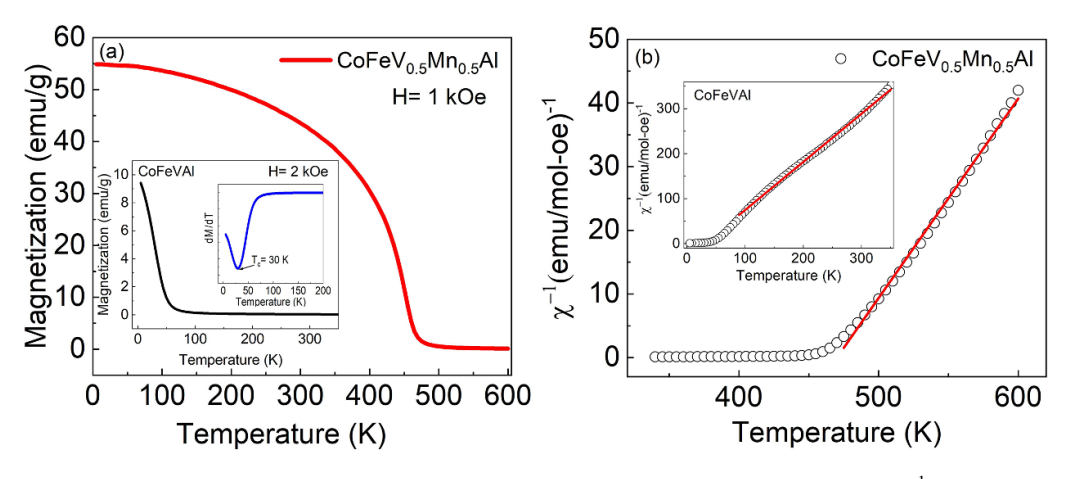


Figure 11. (a) The thermomagnetic curve M(T) and (b) temperature dependence of inverse susceptibility (χ^{-1} vs. T) curve of CoFeV_{0.5}Mn_{0.5}Al alloy. The inset of figure (a) shows both M(T) and dM/dT versus T and the inset of figure (b) shows (χ^{-1} vs. T) of CoFeVAl.

a function of temperature (χ^{-1} vs. T), which is shown in figure 11(b) and its inset. The linear portions of the curves nicely follow the Curie–Weiss law $\chi^{-1} = \frac{T}{C} - \frac{\theta_{\rm CW}}{C}$, where C (emu K mol $^{-1}$) and $\theta_{\rm CW}$ (K) are the Curie constant and Curie–Weiss temperature. The numerical values of the slopes and intercepts of the curves obtained from the curves are 1.07 and -32.6 ± 1.6 , and 0.31 and -147.2 ± 2.2 for CoFeVAl and CoFeV $_{0.5}$ Mn $_{0.5}$ Al, respectively. The values of $\theta_{\rm CW}$ estimated from the intercept of the plots are 35 ± 2 K and 472 ± 7 K for CoFeVAl and CoFeV $_{0.5}$ Mn $_{0.5}$ Al, respectively. These values agree well with the Curie temperatures estimated from the corresponding dM/dT versus T curves. We used these fitting parameters to determine the effective magnetic moment per formula unit using $\mu_{\rm eff} = \sqrt{8C}\mu_{\rm B}$ [39]. The $\mu_{\rm eff}$ values estimated from the Curie constants for CoFeVAl and CoFeV $_{0.5}$ Mn $_{0.5}$ Al are respectively 2.73 and 5.1 $\mu_{\rm B}/f.u$.

The isothermal magnetizations M(H) of both the CoFeVAl and CoFeV_{0.5}Mn_{0.5}Al alloys measured at 2 K are shown in figure 12. Both the alloys show a soft magnetic behavior with coercivities of less than 30 Oe. The saturation magnetization (M_S) of the parent alloy is 12 emu g⁻¹ $(p_s = 0.40 \ \mu_B/f.u.)$ and that of the Mn doped alloy is 59 emu g⁻¹ $(p_s = 1.95 \ \mu_B/f.u.)$. The experimental value of M_S of the Mn doped alloy is very close to the theoretical value $(2.003 \mu_B/f.u)$, whereas that of the parent alloy is much smaller than the theoretical value $(0.95 \mu_B/f.u)$. From the results given above, the corresponding effective spin moments (given by $p_c = \sqrt{1 + \mu_{\rm eff}^2} - 1$) are $p_c = 1.91 \ \mu_B/f.u$. for the parent alloy and $p_c = 4.2 \ \mu_B/f.u$. for the Mn doped alloy.

The Rhodes–Wohlfarth ratio (RWR) p_c/p_s is unity for ferromagnets with ideal localized moments and greater than 1 for itinerant-moment ferromagnets [40]. For weak itinerant ferromagnets, e.g. $ZrZn_2$, $p_c/p_s\gg 1$. The RWR for CoFeVA1 is 4.8 and for CoFeV_{0.5}Mn_{0.5}Al the RWR = 2.15. Thus, the Mn doping significantly decreases the RWR and increases the Curie temperature, leading to a strong ferromagnet with more highly localized moments. Interestingly, RWR values < 1 have been found in many half-metallic ferromagnets [41]. This

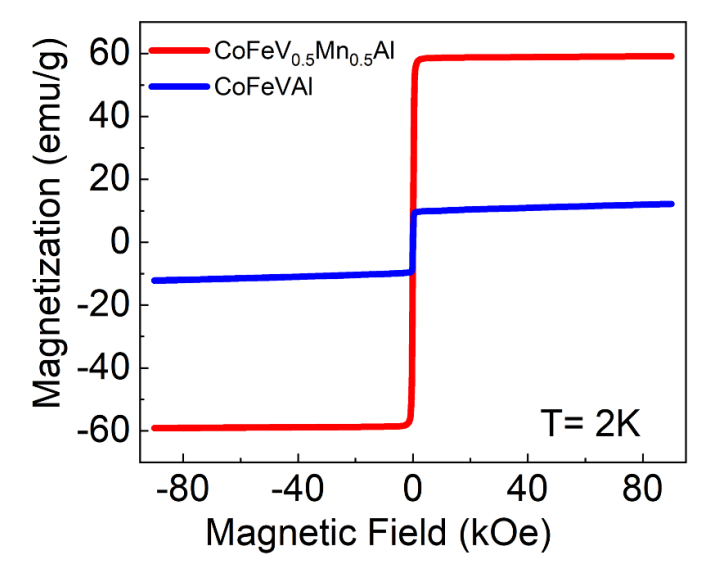


Figure 12. The isothermal magnetization curves of CoFeVAl (blue line) and $CoFeV_{0.5}Mn_{0.5}Al$ (red line) alloys.

is inconsistent with the RWR value of 2.15 we have found for CoFeV_{0.5}Mn_{0.5}Al, which our calculations indicate is halfmetallic. We note that the effective spin moment values (p_c) for both materials are greater than the corresponding calculated moments and the experimental values of saturation moment (p_s) . While there is some structural disorder (B2-type) in the Mn doped alloy, it had minimal impact on the saturation magnetization, which is consistent with the computational results presented above. We conjecture that the enhanced effective moment in the paramagnetic regime of CoFeV_{0.5}Mn_{0.5}Al is due to ferromagnetic short-range order triggered by the atomic disorder. On the other hand, the parent alloy, crystallizing with A2-type disorder, experiences a significant loss in saturation magnetization according to our measurements. This is not consistent with our computational results, which may be due to overlooking certain arrangements of atoms in our simulations of the A2-type disordered cell. Further studies on this issue could shed more light on this discrepancy, but are not pursued in this work, in part because of the smaller practical appeal of CoFeVAl when compared with CoFeV $_{0.5}$ Mn $_{0.5}$ Al, as explained in the text above.

4. Conclusions

In this work, we presented results of a computational and experimental study of CoFeVAl and CoFeV_{0.5}Mn_{0.5}Al Heusler alloys. We demonstrated that while CoFeVAl is not half-metallic due to the presence of a small number of vanadium spin-down states around the Fermi level, it still exhibits a fairly large value of spin polarization (87%) at the equilibrium lattice constant. However, replacing 50% of vanadium with manganese results in an essentially half-metallic transition, largely due to the shift of the Fermi level towards occupied states. In addition, the half-metallicity of CoFeV_{0.5}Mn_{0.5}Al is rather robust in a wide range of considered mechanical strain and B2-type atomic disorder, thus making this alloy potentially suitable for device applications in spin-based electronics. Both considered alloys exhibit ferromagnetic alignment, aside from a small magnetic moment of vanadium which is anti-aligned with the moments of Co and Fe (and Mn in CoFeV_{0.5}Mn_{0.5}Al). Both the alloys synthesized in the bulk form using arc-melting and annealing crystallized in a partially disordered cubic structure. The magnetic properties of the Mndoped sample are in excellent agreement with the theoretical prediction, while the measured and calculated magnetization values of the parent alloy do not agree with each other; further studies may be needed to explain this discrepancy. We hope that the results presented here may be of interest for researchers working on practical applications in spin-based electronics.

Data availability statement

The data that support the findings of this study are available upon reasonable request from the authors.

Acknowledgments

This research is supported by the National Science Foundation (NSF) under Grant Numbers 2003828 and 2003856 via DMR and EPSCoR. This work used the Extreme Science and Engineering Discovery Environment (XSEDE), which is supported by National Science Foundation Grant Number ACI-1548562. This work used the XSEDE Regular Memory (Bridges 2) and Storage (Bridges 2 Ocean) at the Pittsburgh Supercomputing Center (PSC) through allocation TGDMR180059 and the resources of the Center for Functional Nanomaterials, which is a US DOE Office of Science Facility and the Scientific Data and Computing Center, a component of the Computational Science Initiative, at Brookhaven National Laboratory (BNL) under Contract No. DE-SC0012704. Mohd Anas is supported by DOE EPSCoR (DE-SC0024284) grant.

ORCID iDs

Parashu Kharel https://orcid.org/0000-0001-7133-0718
Matthew Wieberdink https://orcid.org/0009-0005-1698-2226

Pavel V Lukashev https://orcid.org/0000-0002-2551-5954

References

- [1] Nelson A, Kharel P, Huh Y, Fuglsby R, Guenther J, Zhang W, Staten B, Lukashev P, Valloppilly S and Sellmyer D J 2015 J. Appl. Phys. 117 153906
- [2] Şaşıoğlu E, Sandratskii L M and Bruno P 2005 Phys. Rev. B 72 184415
- [3] Kurt H, Rode K, Venkatesan M, Stamenov P and Coey J M D 2011 Phys. Status Solidi B 248 2338
- [4] Winterlik J et al 2012 Adv. Mater. 24 6283
- [5] Galanakis I 2016 Heusler Alloys (Springer Series in Materials Science) vol 222, ed C Felser and A Hirohata (Springer)
- [6] Velev J P, Dowben P A, Tsymbal E Y, Jenkins S J and Caruso A N 2008 Surf. Sci. Rep. 63 400
- [7] de Groot R A, Mueller F M, van Engen P G and Buschow K H J 1983 Phys. Rev. Lett. 50 2024
- [8] Galanakis I, Dederichs P H and Papanikolaou N 2002 Phys. Rev. B 66 174429
- [9] Balke B, Fecher G H, Winterlik J and Felser C 2007 Appl. Phys. Lett. 90 152504
- [10] Hanssen K, Mijnarends P, Rabou L and Buschow K 1990 Phys. Rev. B 42 1533
- [11] van Roy W, Wojcik M, Jdryka E, Nadolski S, Jalabert D, Brijs B, Borghs G and De Boeck J 2003 Appl. Phys. Lett. 83 4214
- [12] Katsnelson M, Irkhin V, Chioncel L, Lichtenstein A I and de Groot R A 2008 Rev. Mod. Phys. 80 315
- [13] Elphick K, Frost W, Samiepour M, Kubota T, Takanashi K, Sukegawa H, Mitani S and Hirohata A 2021 Sci. Technol. Adv. Mater. 22 235
- [14] Tavares S, Yang K and Meyers M 2023 *Prog. Mater. Sci.* **132** 101017
- [15] Wang X L 2008 Phys. Rev. Lett. 100 156404
- [16] Lukashev P et al 2016 Appl. Phys. Lett. 108 141901
- [17] Dhakal R, Nepal S, Galanakis I, Adhikari R P and Kaphle G C 2021 J. Alloys Compd. 882 160500
- [18] Gao Q, Opahle I and Zhang H 2019 *Phys. Rev. Mater.* **3** 024410
- [19] Ristoiu D, Nozières J P, Borca C N, Borca B and Dowben P A 2000 Appl. Phys. Lett. 76 2349
- [20] Zhu W, Sinkovic B, Vescovo E, Tanaka C and Moodera J S 2001 Phys. Rev. B 64 R060403
- [21] Galanakis I 2002 J. Phys.: Condens. Matter 14 6329
- [22] Ležaic M, Galanakis I, Bihlmayer G and Blügel S 2005 *J. Phys.: Condens. Matter* 17 3121
- [23] Kharel P et al 2017 AIP Adv. 7 056402
- [24] O'Leary E, Ramker A, VanBrogen D, Dahal B, Montgomery E, Poddar S, Kharel P, Stollenwerk A and Lukashev P 2020 J. Appl. Phys. 128 113906
- [25] Tutic I, Herran J, Staten B, Gray P, Paudel T, Sokolov A, Tsymbal E and Lukashev P 2017 J. Phys.: Condens. Matter 29 075801
- [26] Stuelke L, Margaryan L, Kharel P, Shand P and Lukashev P 2022 J. Magn. Magn. Mater. 553 169267
- [27] de Wijs G A and de Groot R A 2001 *Phys. Rev.* B **64** 020402(R)
- [28] Debernardi A, Peressi M and Baldereschi A 2003 Mater. Sci. Eng. C 23 743
- [29] Prophet S, Dalal R, Kharel P and Lukashev P 2019 J. Phys.: Condens. Matter 31 055801

- [30] Herran J, Carlile R, Kharel P and Lukashev P 2019 *J. Phys.:* Condens. Matter 31 495801
- [31] Kresse G and Joubert D 1999 Phys. Rev. B 59 1758
- [32] Blöchl P 1994 Phys. Rev. B 50 17953
- [33] Perdew J P, Burke K and Ernzerhof M 1996 *Phys. Rev. Lett.* 77 3865
- [34] Methfessel M and Paxton A T 1989 *Phys. Rev.* B **40** 3616
- [35] MedeA-2.22 2017 (Materials Design Inc.)
- [36] Towns J et al 2014 XSEDE: accelerating scientific discovery Comput. Sci. Eng. 16 62–74
- [37] Rodriguez-Carvajal J 1990 FULLPROF: a program for Rietveld refinement and pattern matching analysis Abstracts of the Satellite Meeting on Powder Diffraction of the XV Congress of the IUCr (Toulouse, France) p 127
- [38] Takamura Y, Nakane R and Sugahara S 2009 *J. Appl. Phys.* **105** 07B109
- [39] Mugiraneza S and Hallas A M 2022 Commun. Phys. 5 95
- [40] Wohlfarth E P 1978 J. Magn. Magn. Mater. 7 113
- [41] Otto M, van Woerden R, van der Valk P, Wijngaard J, van Bruggen C, Haas C and Buschow K 1989 *J. Phys.:* Condens. Matter 1 2341